

## Yeni Bir Schiff Bazı Molekülüne *in Siliko* Tıbbi ve Hesaplamalı Yöntemlerle Bir Bakış

Songül ŞAHİN<sup>1\*</sup>, Necmi DEGE<sup>2</sup>

<sup>1</sup> Ondokuz Mayıs University, Faculty of Sciences, Department of Chemistry, Samsun, Turkey.

<sup>2</sup> Ondokuz Mayıs University, Faculty of Sciences, Department of Physics, Samsun, Turkey.

Corresponding author\* e-mail: [songul.sahin@omu.edu.tr](mailto:songul.sahin@omu.edu.tr). ORCID ID: <https://orcid.org/0000-0003-4713-3137>  
necmid@omu.edu.tr. ORCID ID: <https://orcid.org/0000-0003-0660-4721>

Geliş Tarihi: 19.01.2023 Kabul Tarihi: 10.08.2023

### Öz

Bu çalışmada yeni bir Schiff bazı molekülünün, (*E*)-1-(5-nitro-2-(piperidin-1-yl) phenyl)-*N*-(4-phenoxyphenyl) methanimine, sentezi ve karakterizasyonu amaçlandı. Bunun yanı sıra bu molekülün moleküler yüzey alanı, kristal yapısı, moleküler arası kuvvetleri, elektronik ve spektroskopik özellikleri araştırıldı. Ayrıca SARS-CoV-2 ana proteazının (Mpro) aktif yerleri üzerinde kenetleme deneyleri gerçekleştirildi ve sonuç yerli ligand N3 inhibitörünün etkinliği ile kıyaslandı. Başlık molekülü için ana bulgular aşağıdaki gibi özetlenebilir: Uzay grubu P-1'dir ve triklinik sistemde kristallenir. Birim hücre iki monomerik birimden oluşur. Molekülde güçlü elektrofilik saldırı pozisyonları vardır ama nükleofilik merkezler düşük etkinliktedir. FMO analizine göre, başlık bileşiği yumuşak, kinetik ve kimyasal olarak kararsız ve oldukça reaktif bir malzemedir. Moleküler kenetleme deneylerine göre, bağlanma serbest enerjisinin hesaplanan değeri (-9.28 kcal/mol) yerli inhibitörün değerinden (-7.11 kcal/mol) daha düşüktür ve bu yüzden başlık bileşiği SARS-CoV-2 ana proteazi için potansiyel bir inhibitör adayı olarak düşünülebilir.

### Anahtar kelimeler

MEP; HOMO-LUMO;  
SARS-CoV-2; Schiff bazı

## A Perspective with *in Silico* Medicinal and Computational Methods to A New Schiff Base Molecule

### Abstract

In this study, the synthesis and characterization of a new Schiff base molecule, (*E*)-1-(5-nitro-2-(piperidin-1-yl) phenyl)-*N*-(4-phenoxyphenyl) methanimine, were aimed. In addition, the molecular surface area, crystalline structure, intermolecular forces, electronic and spectroscopic properties of the molecule were investigated. Docking studies were also performed on the active sites of the main protease (Mpro) of SARS-CoV-2, and the docking result was compared with the efficacy of the native ligand N3 inhibitor. The main findings for the title molecule can be summarized as follows: The space group is P-1 and it crystallizes in the triclinic system. The unit cell consists of two monomeric units (Z=2). There are strong electrophilic attack sites in the molecule, but nucleophilic centers have low efficiency. According to the FMO analysis, the title compound is a soft, kinetically and chemically unstable and highly reactive material. The value of the binding free energy calculated by docking experiments (-9.28 kcal mol<sup>-1</sup>) is lower than that of the native inhibitor (-7.11 kcal/mol) and thus can be considered as a potential inhibitor candidate for the main protease of SARS-CoV-2.

### Keywords

MEP; HOMO-LUMO;  
SARS-CoV-2; Schiff  
base

© Afyon Kocatepe Üniversitesi

### 1. Introduction

In December 2019, the first case of the outbreak called COVID-19 was reported in the Wuhan province of China (Sheikhpour, 2020; Faisal *et al.*, 2021; Srivastava *et al.*, 2021). After the first reported case in China, other cases and death news

were heard from over the world. On 11 February 2020, the name of the novel coronavirus (2019 nCoV) that causes coronavirus disease (COVID-19) was changed as SARS-CoV-2 by the ICTV (Xiang *et al.*, 2021). On 11 March 2020, the WHO announced the epidemic as a pandemic (Xiang *et al.*, 2021). Finally, with the up-to-date data from the WHO coronavirus

dashboard (access date 08.11.2022; <https://covid19.who.int/>), 629 370 889 cumulative cases and 6 578 245 deaths were globally reported (WHO).

The clinical symptoms of the disease have changed from asymptomatic to severe symptoms (Dömling and Gao, 2020). The main clinical findings in coronavirus patients are fever, dry cough (Gao *et al.*, 2021; Shagufta and Ahmad, 2021; Xiang *et al.*, 2021), fatigue, dyspnea (Gao *et al.*, 2021; Xiang *et al.*, 2021), tiredness (Shagufta and Ahmad, 2021). The more severe ones are sepsis or septic shock, multiple organ failure (Gao *et al.*, 2021; Xiang *et al.*, 2021), secondary infections (Xiang *et al.*, 2021), acute respiratory distress syndrome, coagulation dysfunction (Gao *et al.*, 2021). The mortality rate (3-5%) in COVID-19 is lower than other coronavirus families include SARS-CoV (9-15%) and MERS-CoV (34-37%) (Gao *et al.*, 2021; Shagufta and Ahmad, 2021). However, senescence and comorbidities are high-risk factors in COVID-19 (Shagufta and Ahmad, 2021), and older people are responsible for 80% of hospitalizations (Mueller *et al.*, 2020). The spreading rate of the novel coronavirus member (SARS-CoV-2) in the community is also higher than the SARS and MERS (Petrosillo *et al.*, 2020).

Among the various druggable targets of SARS-CoV-2 (Artese *et al.*, 2020; Amin *et al.*, 2021), Mpro and PLpro play particularly important roles in viral entry, host cell invasion (Faheem *et al.*, 2020), viral replication (Sohag *et al.*, 2020), enzymatic activity (Amin *et al.*, 2021). Hence, targeting these druggable targets is among the critical strategies to antiviral drug design and inhibit viral activation.

Various repurposed drugs have been used to treat coronavirus disease. Some of them are remdesivir, favipiravir, hydroxychloroquine, lopinavir/ritonavir (Awadasseid *et al.*, 2021; Mandal *et al.*, 2021), nafamostat mesylate, azithromycin (Awadasseid *et al.*, 2021). Remdesivir (GS-5734) is a nucleotide analog drug, and the FDA has approved its urgent use authorization to treat COVID-19 (Awadasseid *et al.*, 2021; Young *et al.*, 2021). Positive antiviral effect of remdesivir has been reported in animal models against SARS-CoV and MERS-CoV (Sheahan *et al.*,

2017; Awadasseid *et al.*, 2021), the antiviral activity of remdesivir towards SARS-CoV-2 has been reported both in vitro and in vivo studies (Frediansyah *et al.*, 2021). As a result of global efforts to find a vaccine, many vaccine candidates (more than 292) have been investigated. Only a few vaccines, such as Pfizer/BioNTech, Moderna, Johnson & Johnson, AstraZeneca/Oxford, have been approved for urgent use in treating COVID-19 disease. Their efficacy values and the recommended using age differ from each other. Among these vaccines, Pfizer/BioNTech has the most remarkable efficacy (95%) and the lowest use age (16 years and above) (Alshrari *et al.*, 2021). However, despite the many efforts to cure coronavirus disease, no specific drugs have been discovered to fight COVID-19. The disease's threatening effect continues; therefore, there is an urgent need to develop better therapeutic antiviral drugs or broad-spectrum inhibitors to combat the deadly disease.

This study reports the synthesis of a new molecule and investigations its structural characteristics. Comparative docking studies were performed between the synthesized molecule and reference inhibitor N3 on the Mpro of SARS-CoV-2. Docking results have showed the binding energy score of the title compound is lower than the reference inhibitor.

## **2. Materials and Methods**

### **2.1 Materials**

Chemicals: 5-nitro-2-(piperidin-1-yl)benzaldehyde; 4-phenoxyaniline; ethanol.

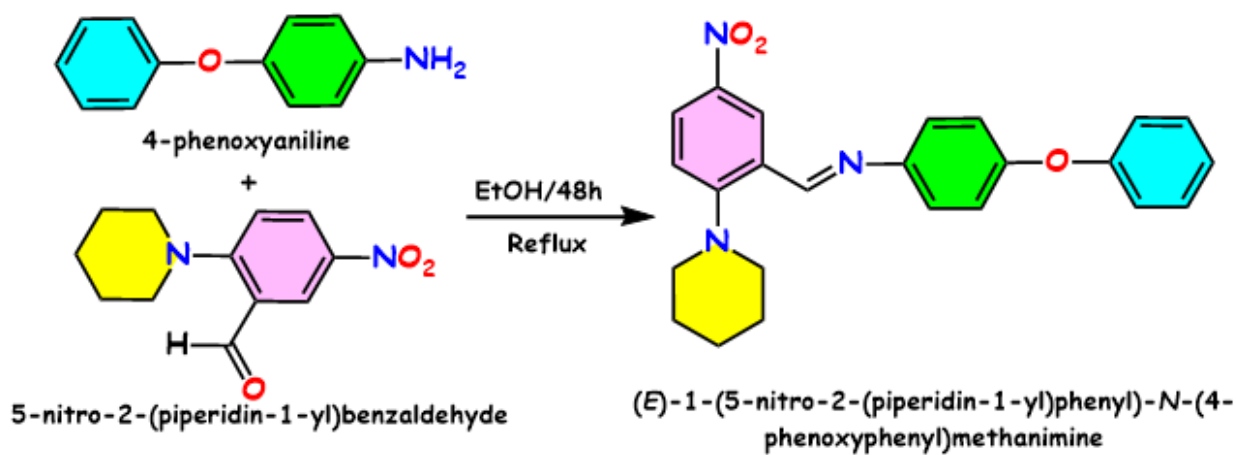
X-Ray and computational analysis: SHELXT (Sheldrick, 2015), SHELXL (Sheldrick, 2015), PubCIF (Westrip, 2010), Gaussian 03 (Frisch *et al.*, 2009)-DFT (Parr, 1980), Crystal Explorer (Turner *et al.*, 2017), Mercury (Macrae *et al.*, 2006).

Docking experiments: AutoDock4 and AutoDockTools4 (Morris *et al.*, 2009)/molecular docking; PDB (Berman *et al.*, 2000)/3D structure of protein-ligand complex; PLIP (Salentin *et al.*, 2015)/secondary interactions and species.

## 2.2 Synthesis method

The synthesis scheme of the title compound was drawn in Scheme 1. The equivalent amounts of an aldehyde (8 mg, 0.034 mmol) and amine (6.3 mg, 0.034 mmol) were combined and solved in 25 mL of ethanol. The reaction mixture was heated up to the reflux temperature. TLC was used to follow up the reaction process using a mobile phase composed of the mixture of hexane and ethyl acetate (the ratio, 95:5). The crystallization solvent, CH<sub>3</sub>CH<sub>2</sub>OH, was

vaporized by the slow evaporation technique. The formed crystals were used in the X-Ray and other analyses. Melting point: 190-192 °C. Yield: 82% (11.19 mg). C<sub>24</sub>H<sub>23</sub>N<sub>3</sub>O<sub>3</sub>. Molecular weight: 401.45 g/mol. FTIR (ATR),  $\nu/\text{cm}^{-1}$ : 3084, 3050 (Ar. C-H); 2940, 2857 (Al. C-H); 2816 (CH=N); 1582 (C=N); 1483, 1446 (Ar. C=C); 1500, 1328 (NO<sub>2</sub>); 1231, 1175, 1155, 1130, 1076, 1024 (C-N; C-O) (Figure 1/top). UV-Vis (in ethanol, 1.0x10<sup>-4</sup> M),  $\lambda_{\text{max}}/\text{nm}$  (log $\epsilon$ ): 362 (4.05) (Figure 1/bottom).



Scheme 1. The synthesis route for the title compound

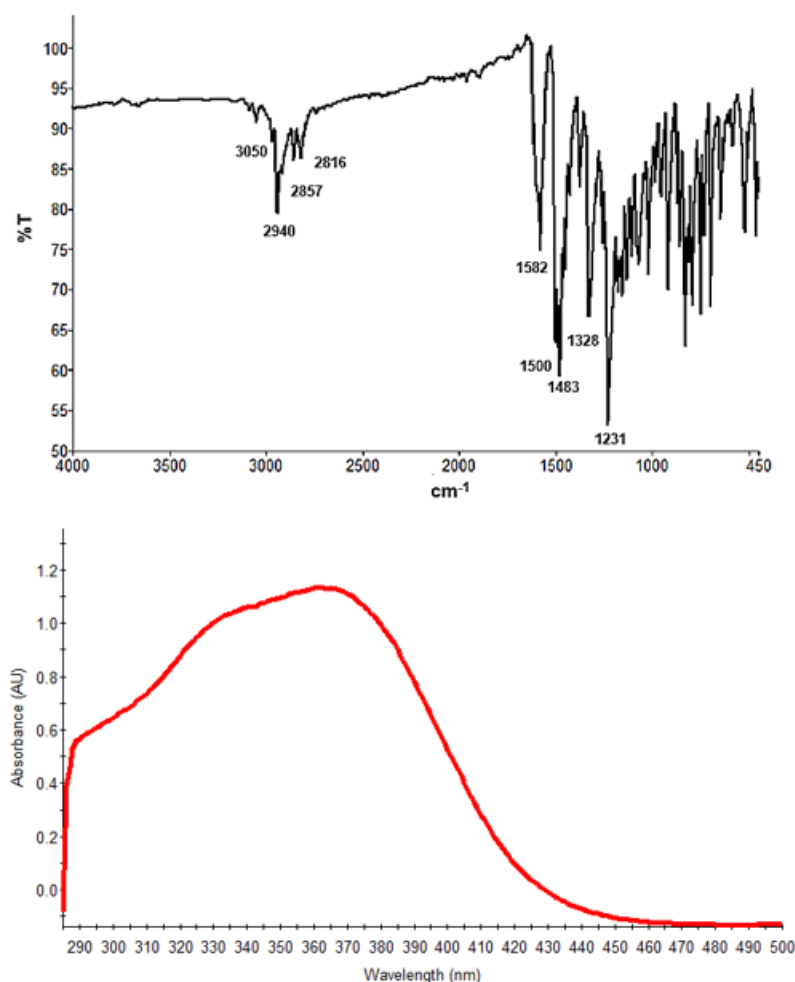


Figure 1. FTIR (top) and UV-Vis (bottom) spectra of title compound

### 3. Results and Discussion

#### 3.1. Crystallographic, structural, and geometrical parameters

The crystal data were collected with the Apex II Quazar three-circle diffractometer at 299 K. The crystal structure was solved by the SHELXT program. All refinements were performed using the SHELXL program via the full-matrix least-squares on the F2 method. The crystal dimensions were measured as 0.23, 0.17, 0.07 mm<sup>3</sup>. The newly synthesized molecule is represented by the name of (*E*)-1-(5-nitro-2-(piperidin-1-yl) phenyl)-*N*-(4-phenoxyphenyl) methanimine, C<sub>24</sub>H<sub>23</sub>N<sub>3</sub>O<sub>3</sub> formula, triclinic system, and P -1 space group. The unit cell deposits two monomeric molecules in the crystal system. Unit cell dimensions are different; the lengths are 8.135 (a), 10.459 (b), 12.285 (c), and the

angles are 106.32 ( $\alpha$ ), 96.72 ( $\beta$ ), 94.80 ( $\gamma$ ). The crystal structure's CCDC deposition number is 2120420, <https://www.ccdc.cam.ac.uk/>. The title molecule comprises four rings, including three aromatic rings and one aliphatic ring; it bears six heteroatoms, including three oxygens and three nitrogens. The main organic groups in the title molecule are diphenyl ether, nitro benzyl, piperidinyl, and imine. The molecule's aromatic and aliphatic C-H bond lengths have been measured as 0.93 and 0.97 Å. The aromatic (double bond) and aliphatic (single bond) C-C bond lengths have changed between 1.355 (C18-C23) and 1.407 Å (C6-C11) (aromatics) and 1.486 (C2-C3) and 1.503 Å (C3-C4) (aliphatics). Imine bond (C24-N3) length is 1.258 Å. The carbon-nitrogen single bonds have changed between 1.380 (N2-C6) (in which nitrogen bonded to aromatic ring carbon) and 1.454 (N2-C5) Å (in

which nitrogen bonded to aliphatic ring carbon). The N=O bond lengths in the nitro group are 1.204 (N1-O3) and 1.208 (N1-O2) Å. The C-O bond lengths among the two phenyl rings (R3 and R4 in Figure 2) are 1.364 (O1-C15) and 1.376 Å (O1-C18). Some specific bond angles are those: O2-N1-O3 (122.73), C20-C19-C18 (119.30), C14-C15-C16 (120.16), C9-C8-C7 (119.58), C3-C2-C1 (111.67), C24-N3-C12 (119.47), C18-O1-C15 (118.71). The formed intermolecular hydrogen bonds in the molecule are

greater than 2.5 Å and have been listed in Figure 2b and Table 1. Figure 2b also shows the other secondary interacted atom's list in the crystal packaging. Figure 2a and Figure 2c show the molecule's numbered model and crystal growing points, respectively. A section from the supramolecular crystalline framework of the molecule has been shown in Figure 3.

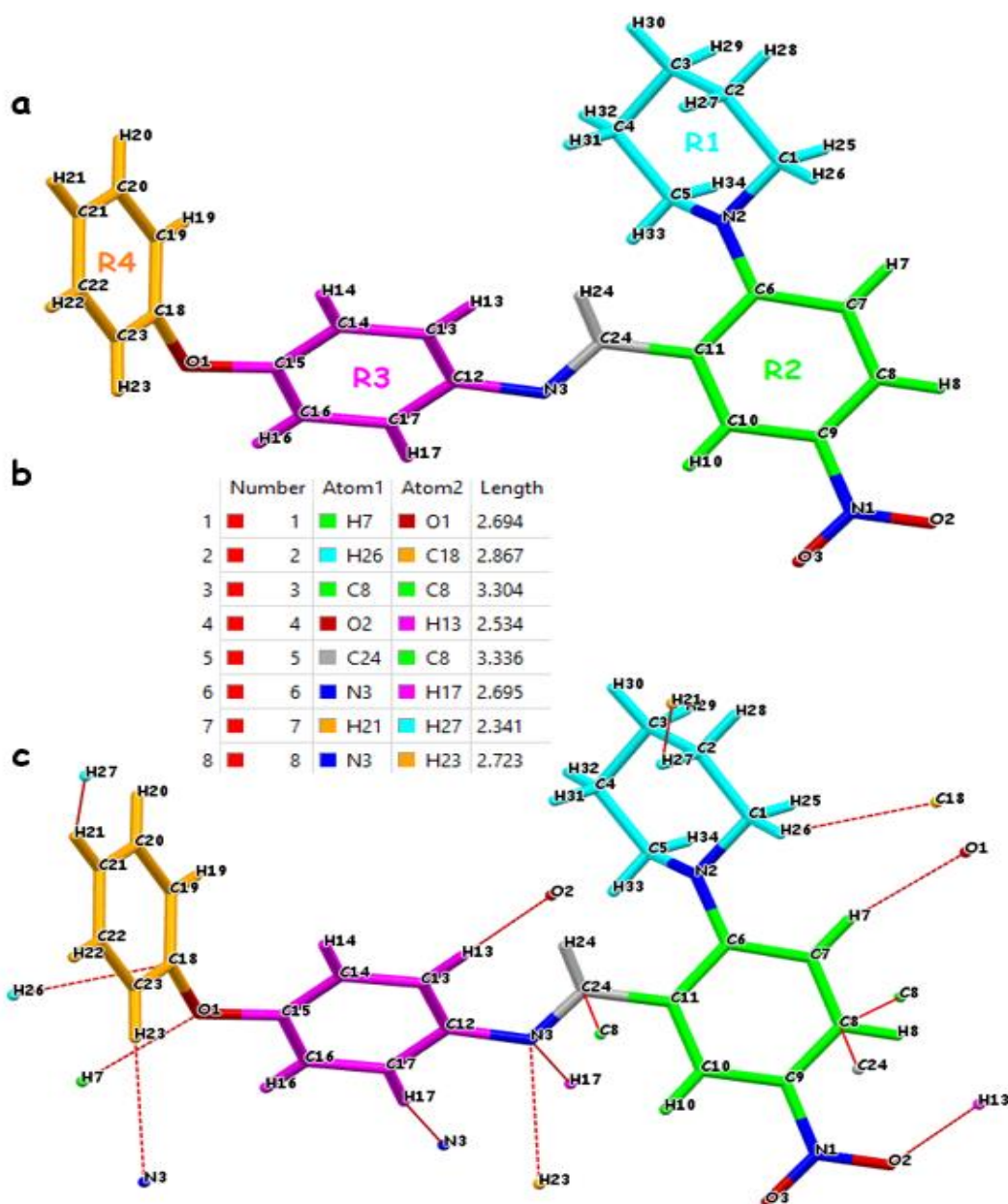


**Figure 2.** 3D numbered stick model of the title compound (a); bond lengths table for secondary interactions in the crystal packaging (b); the crystal growth points/shown with the red dashed line

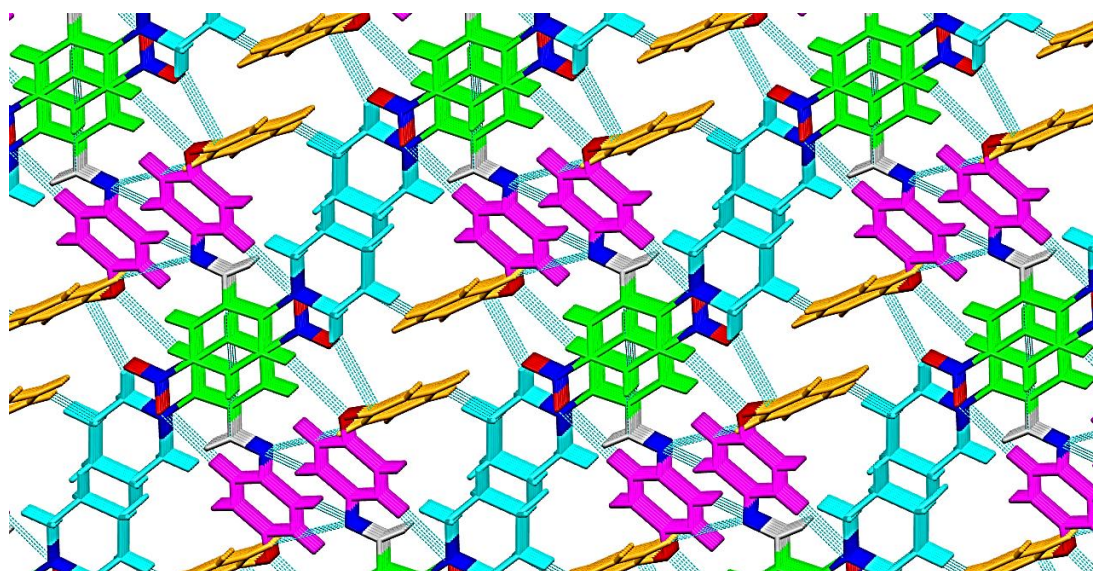


Figure 3. A section of crystal structure packaging

Table 1. The hydrogen bond list and bond geometry (Å, °) for the title compound

| D—H...A      | D—H  | H...A | D...A     | D—H...A |
|--------------|------|-------|-----------|---------|
| C17—H17...N3 | 0.93 | 2.69  | 3.567 (4) | 156     |
| C13—H13...O2 | 0.93 | 2.53  | 3.443 (5) | 166     |

### 3.2. Molecular electrostatic potential (MEP) and Mulliken atomic charges

MEP map is a 3D dimensional surface mapping according to the entire electron density of a molecule. It provides many benefits as understanding molecular shape and size, electron density, relative polarity, nucleophilic and electrophilic zones, molecular interactions (Kumar *et al.*, 2022), chemical reactivity (Raghi *et al.*, 2018). The red, blue, and green colors point out the zones in which electrostatic potential is most negative, zero, and the most positive, respectively. Red and yellow regions are exposed to electrophilic attacks, whereas blue and cyan regions are exposed to nucleophilic attacks. In the present study, the MEP map of the topic compound (Figure 4) has been calculated using the DFT/B3LYP method and 6-31 G (d, p) basis set in Gaussian software. Figure 4 shows the MEP maps of the molecule with the solid surface

(a), mesh surface (b), and semi-opened surface (c). We can conclude these presumptions about the molecule from the MEP and Mulliken charges: • The red surfaces occupy O1, O2, O3, and N2 atoms, so these atoms or regions open to interactions with the electrophilic species or groups. • In the MEP, there are no deepest blue surfaces, so the molecule hasn't got strong nucleophilic positions. But the cyan regions occupy some groups (especially hydrogens) in the piperidiny ring (R1 ring in Figure 2). These groups can be open to weak interactions with the nucleophilic species. • The top negatively charged five atoms are O1 (-0.587), N2 (-0.557), N3 (-0.525), O2 (-0.448), O3 (-0.446); the top positively charged five atoms are N1 (0.398), C15 (0.310), C6 (0.274), C18 (0.272), C9 (0.248). The positive charge density is relatively lower than the negative charge density in Mulliken atomic charge values; that is why the absence of strong nucleophilic positions in the molecule.

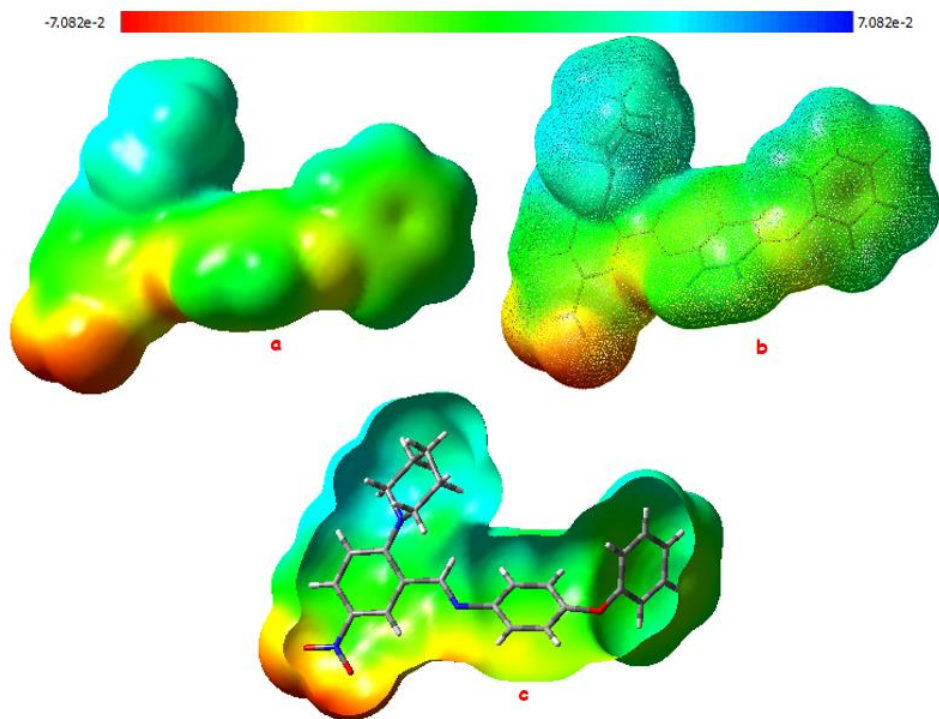


Figure 4. MEP maps for the title compound; solid surface (a), transparent surface (b), semi-opened surface (c)

### 3.3. Molecular orbital analysis and chemical descriptors

Frontier molecular orbitals (FMOs), HOMO and LUMO orbitals, play a critical role in quantum chemistry regarding understanding chemical reactivity and kinetic stability in the molecules (Shukla *et al.*, 2014). While the HOMO orbital is represented by electron donor ability or ionization potential, the LUMO orbital is represented by electron acceptor ability or affinity (Azhagiri *et al.*, 2014). The lower value of FMOs energy gap is associated with more polarizability, high chemical reactivity, low kinetic stability, and softness of a molecule, and vice versa. The HOMO and LUMO pictorial representation and their energy values for our compound were calculated by the DFT method and 6-31 G (d, p) basis set. These orbitals are shown in Figure 5. Some crucial global reactivity descriptors were calculated for our compound, the

calculated HOMO energy is -5.621 eV, the LUMO energy is -2.125 eV, and the energy gap value between these orbitals is 3.496 eV. The calculations, pictogram, and global reactivity descriptors clearly show that

- The small energy gap value (3.496 eV) signs out easy molecular electrical transport, lower chemical stability, high chemical reactivity, softness, easy polarizability, low kinetic stability in the molecule.
- While the HOMO orbitals localized in the almost entire molecule, the LUMO orbitals localized in the R2 ring, and nitro atoms bonded to the R2 aromatic ring.
- High electronegativity (3.873) and small hardness value (1.748) show the molecular instability.
- Low softness (0.286) and high electrophilicity index (4.290) of the molecule are related to decreased toxicity and good biological activity.
- $\Delta N_{max}$  (2.215) accounts for the maximum charge that an electrophilic species may accept from a molecule.

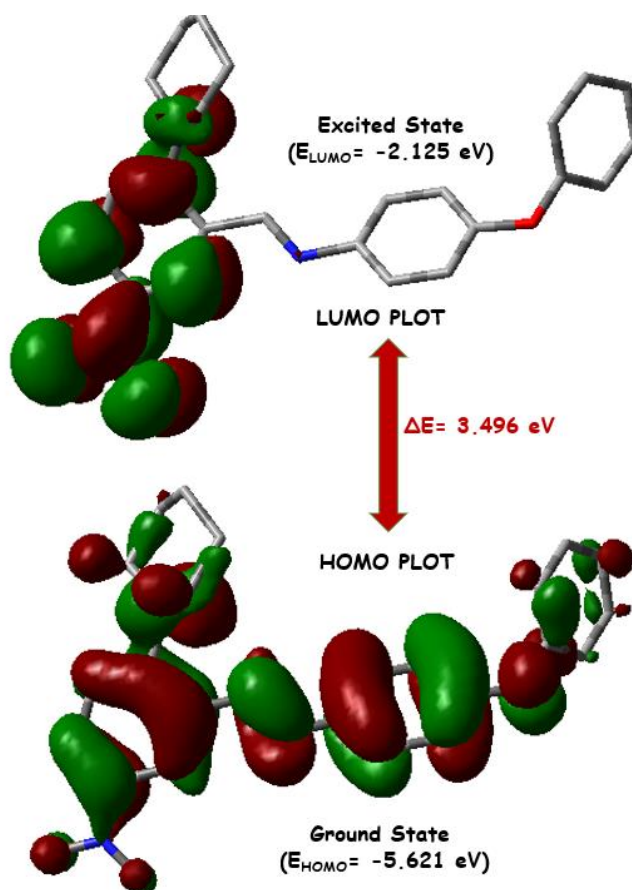


Figure 5. HOMO and LUMO orbitals and their energies for the topic molecule

### 3.4. Hirshfeld surfaces and fingerprint analysis

The analyses in the title were performed to get information about intermolecular interactions and their contributions. The CIF file of the crystal structure was inputted into the Crystal Explorer software. Various Hirshfeld surfaces, including dnorm, di, de, shape index, curvedness, fragment patch, and whole fingerprint plot, were produced and illustrated in Figure 6 and 7. Dnorm surface is helpful to uncover the close interactions. The bright and large red zones on the dnorm surface show the place of the hydrogen bonding interactions. These areas for our compound were shown with the yellow circles in which the signed atoms form the hydrogen bonds. Because the hydrogen bond distance between H17 and N3 is longer than H13

and O2, the red points on H17 and N3 atoms are not large and were not signed. In the shape index Hirshfeld surface, the adjacent blue/red triangles (shown in the red circle) are the significant indicator for the presence of  $\pi$ - $\pi$  stacking interactions in the molecule. The quantitative results of the intermolecular interactions are shown in Figure 6 with the pie chart. The H...H interactions have the highest contribution of 48.90%; the second chief contribution has O...H interactions with a value of 20.10%. The third contribution is 19.60% and belongs to the C...H interactions. The contribution of N...H interactions is 5.10%, and the others have a ratio of 6.80%.

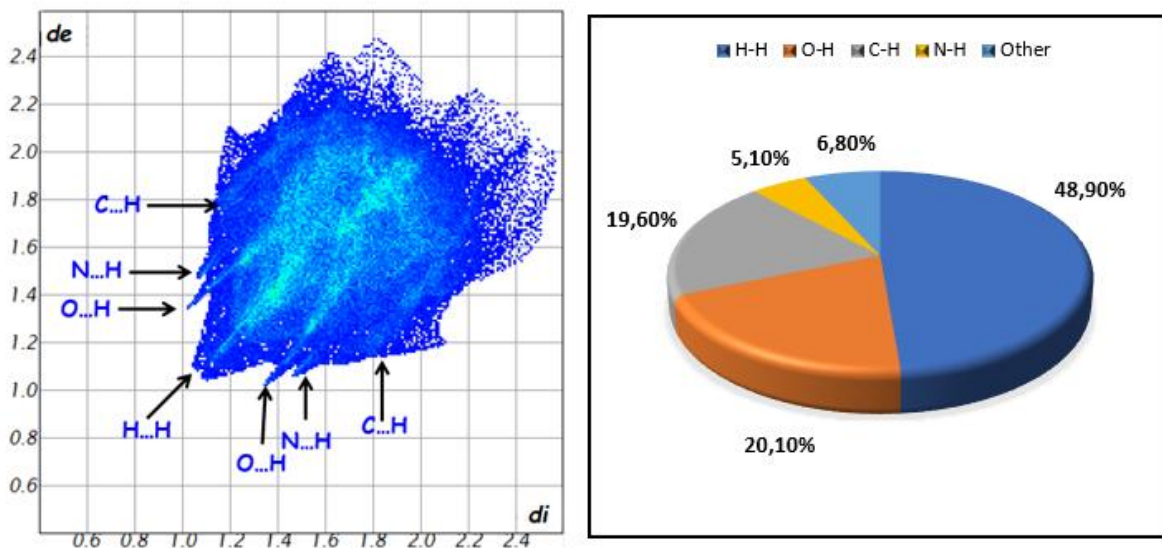


Figure 6. The fingerprint analysis (left) and percent contribution analysis of the intermolecular interactions (right)

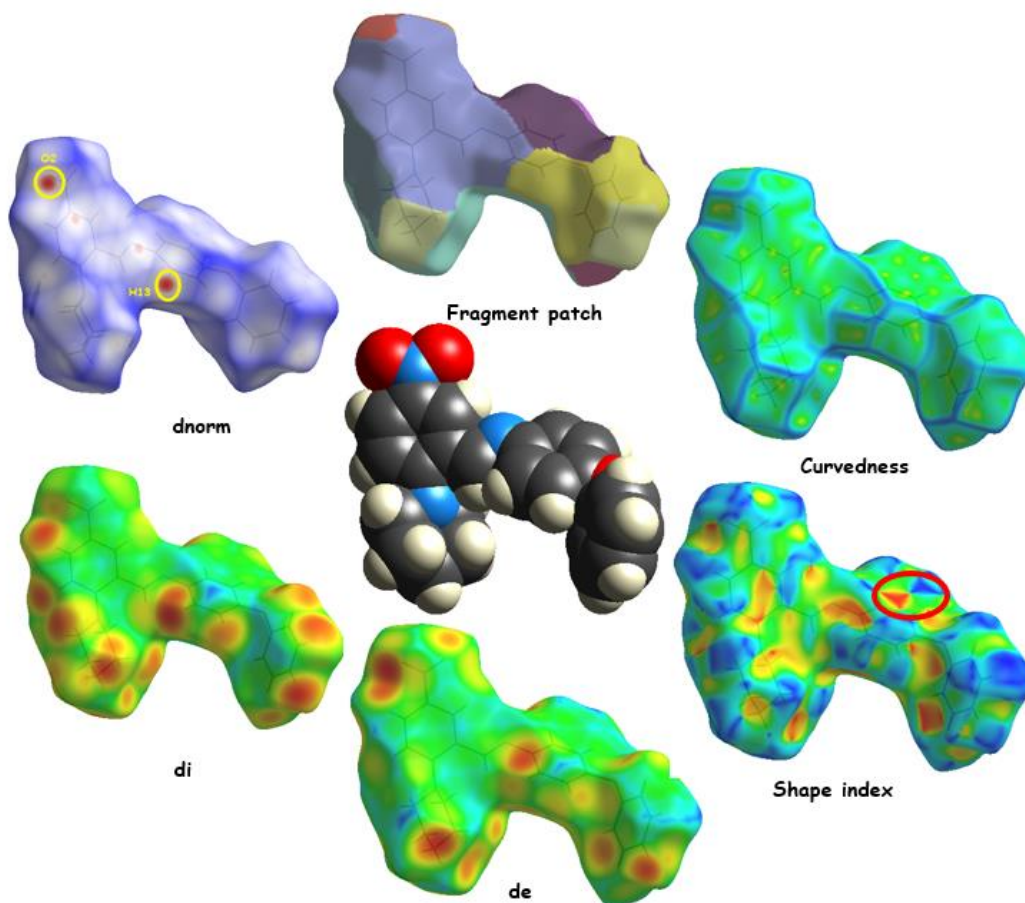
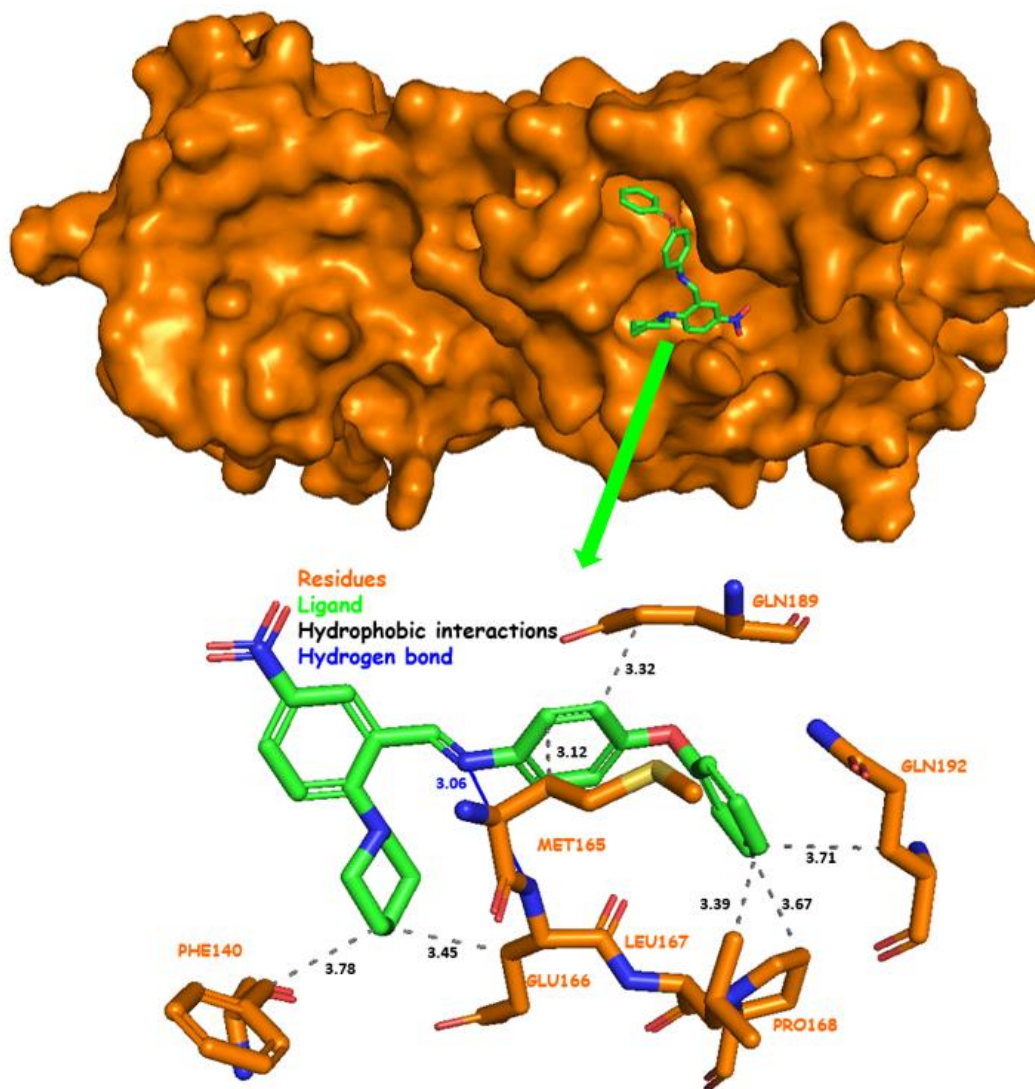


Figure 7. Hirshfeld surfaces of the topic molecule

### 3.5. Docking studies

Molecular docking plays a vital role in computational drug discovery and helps determine the interactions between a small molecule and a target protein. In this way, it is possible to characterize the binding position of small molecules in the binding site of the target protein or macromolecule and assess the binding affinities (Meng *et al.*, 2011). On this bases, we performed a docking study between our compound and the main protease (Mpro) of SARS-CoV-2. Docking experiments were performed using AutoDock4 and AutoDockTools platforms. The 3D structure of the target protein (Mpro) was provided by the RCSB PDB database (<https://www.rcsb.org/>) with the PDB ID: 6LU7 and 2.16 Å resolution. The title compound was translated into 3D PDB format using the online tool SMILES translator (<https://cactus.nci.nih.gov/translate/>). Before docking experiments, the target structure was prepared by adding Kollman charges and polar hydrogens, deleting water molecules, and minimizing energy. A Lamarckian genetic algorithm was used for the docking experiment. The grid box was arranged into the active sites of Mpro. The spacing of the grid box was chosen to be 0.375 Å.

The grid box was centered in dimensions -13.619, 13.964, and 70.229 for x, y, and z, respectively. The docking pose of the ligand molecule and the whole Mpro surface are shown in Figure 8. The docking experiment was also performed with the reference inhibitor N3, benzyl (3*S*, 6*S*, 9*S*, 12*S*, *E*)-9-isobutyl-6-isopropyl-3-methyl-1-(5-methylisoxazol-3-yl)-1,4,7,10-tetraoxo-12-(((*S*)-2-oxopyrrolidin-3-yl)methyl)-2,5,8,11-tetraazapentadec-13-en-15-oate (Figure 9). AutoDock4 calculated the binding energies of query molecule and inhibitor N3 as -9.28 and -7.11 kcal mol<sup>-1</sup>, respectively. Also, ligand efficiencies and inhibitory constants were calculated at the levels -0.31 and 0.15 µM for query molecule and -0.15 and 6.18 µM for reference inhibitor N3. Hydrophobic interactions and hydrogen bonds between target and query compound were shown in Figure 8, together interacted residues. Green and gold-colored sticks represent the query compound and the interacted residues, respectively. Eight residues on the binding site of Mpro have been joined into complex interactions; one of these interactions is the hydrogen bond between GLU166 and nitrogen atom (N3 in Figure 2) in the imine group, the others are hydrophobic interaction forces.



**Figure 8.** Docking conformation of the query compound in the active sites of the SARS-CoV-2 main protease (Mpro) (top) and the detailed investigation of the query compound interaction map (bottom)

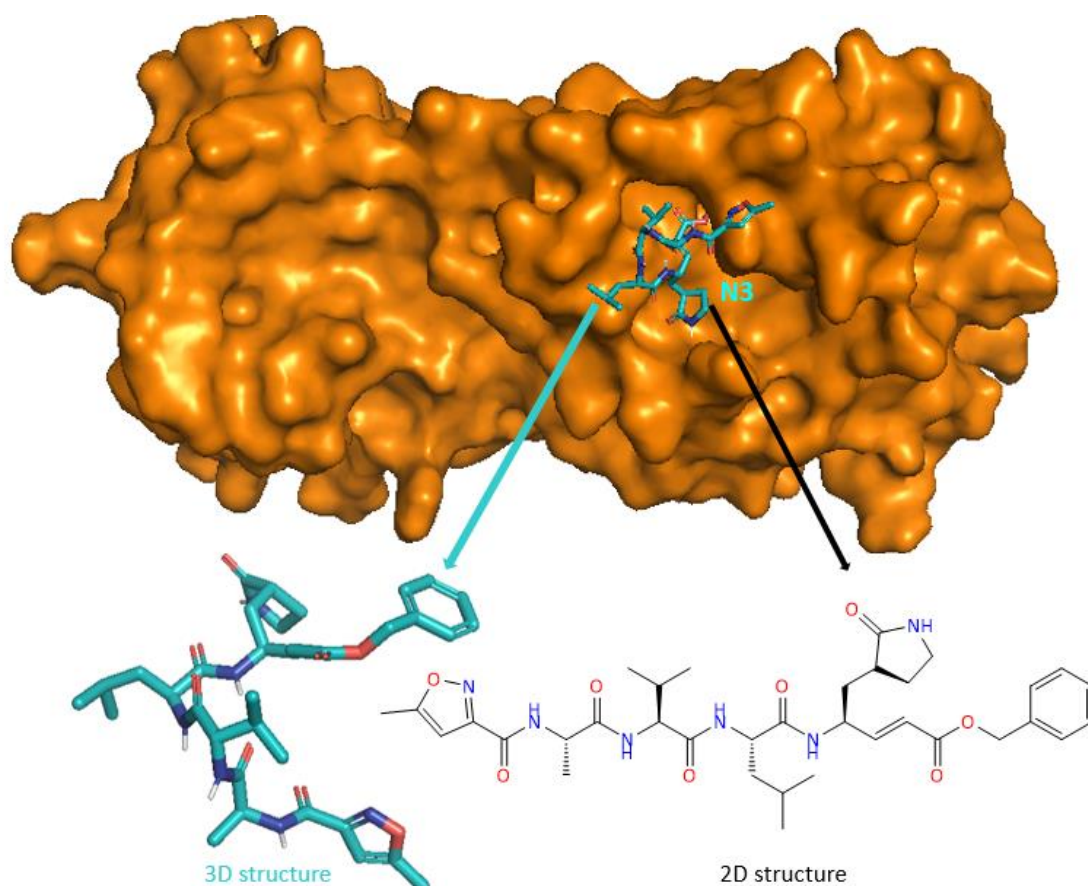


**Figure 9.** Docking conformation of the reference inhibitor N3 in the active sites of the SARS-CoV-2 main protease (Mpro) (top), and 2D and 3D structures of the N3 (bottom)

#### 4. Conclusion

In this work, a new organic compound was synthesized and characterized. Crystallographic, spectroscopic, electronic, and geometric properties were investigated. Besides these, the medicinal chemistry properties of the compound were calculated and evaluated. Antiviral activity prediction on Mpro was performed by molecular docking studies. In a nutshell;

The compound characterized with the  $C_{24}H_{23}N_3O_3$  formula has a triclinic crystal system and P-1 space group. The molecule bears electrophilic centers but has no nucleophilic attack regions; Mulliken charges on atoms have distributed between -0.587 and +0.398. The HOMO energy is -5.621 eV, the LUMO energy is -2.125 eV, and the energy gap is 3.496 eV. Charge transfer is easy, chemical and kinetic stabilities are low. It is a chemically reactive and soft molecule. Hydrogen-hydrogen interactions and hydrogen bonds are important secondary

interactions in crystal packaging and molecular stability. The inhibitory effect of the compound according to free binding energy ( $-9.28 \text{ kcal mol}^{-1}$ ) calculated from docking experiments is lower than reference inhibitor N3 ( $-7.11 \text{ kcal mol}^{-1}$ ). In this concept, the title compound showed excellent antiviral inhibitory activity against Mpro of SARS-CoV-2 compared with the native ligand N3. After computational studies, we evaluate the title compound as a potential antiviral compound. This compound may be used and tested for further experimental studies on antiviral activity.

#### Conflict of Interest

None

#### Supplementary data

CCDC 2120420 contains the supplementary information of the title compound.

## 5. References

- Alshrari, A. S., Hudu, S. A., Imran, M., Asdaq, S. M. B., Ali, A. M., and Rabbani, S. I., 2021. Innovations and development of Covid-19 vaccines: A patent review. *Journal of Infection and Public Health*, **15**, 123-131. DOI: <https://doi.org/10.1016/j.jiph.2021.10.021>.
- Amin, S. A., Banerjee, S., Ghosh, K., Gayen, S., and Jha, T., 2021. Protease targeted COVID-19 drug discovery and its challenges: Insight into viral main protease (Mpro) and papain-like protease (PLpro) inhibitors. *Bioorganic & Medicinal Chemistry*, **29**, 115860. DOI: <https://doi.org/10.1016/j.bmc.2020.115860>.
- Artese, A., Svicher, V., Costa, G., Salpini, R., Di Maio, V. C., Alkhatib, M., Ambrosio, F. A., Santoro, M. M., Assaraf, Y. G., Alcaro, S., and Ceccherini-Silberstein, F., 2020. Current status of antivirals and druggable targets of SARS CoV-2 and other human pathogenic coronaviruses. *Drug resistance updates : reviews and commentaries in antimicrobial and anticancer chemotherapy*, **53**, 100721. DOI: [10.1016/j.drup.2020.100721](https://doi.org/10.1016/j.drup.2020.100721).
- Awadasseid, A., Wu, Y., Tanaka, Y., and Zhang, W., 2021. Effective drugs used to combat SARS-CoV-2 infection and the current status of vaccines. *Biomedicine & Pharmacotherapy*, **137**, 111330. DOI: <https://doi.org/10.1016/j.biopha.2021.111330>.
- Azhagiri, S., Jayakumar, S., Gunasekaran, S., and Srinivasan, S., 2014. Molecular structure, Mulliken charge, frontier molecular orbital and first hyperpolarizability analysis on 2-nitroaniline and 4-methoxy-2-nitroaniline using density functional theory. *Spectrochimica Acta Part A: Molecular and Biomolecular Spectroscopy*, **124**, 199-202. DOI: <https://doi.org/10.1016/j.saa.2013.12.106>.
- Berman, H. M., Westbrook, J., Feng, Z., Gilliland, G., Bhat, T. N., Weissig, H., Shindyalov, I. N., and Bourne, P. E., 2000. The Protein Data Bank. *Nucleic Acids Research*, **28**, 235-242. DOI: [10.1093/nar/28.1.235](https://doi.org/10.1093/nar/28.1.235).
- Dömling, A. and Gao, L., 2020. Chemistry and Biology of SARS-CoV-2. *Chem*, **6**, 1283-1295. DOI: [10.1016/j.chempr.2020.04.023](https://doi.org/10.1016/j.chempr.2020.04.023).
- Faheem, Kumar, B. K., Sekhar, K., Kunjiappan, S., Jamal, J., Balaña-Fouce, R., Tekwani, B. L., and Sankaranarayanan, M., 2020. Druggable targets of SARS-CoV-2 and treatment opportunities for COVID-19. *Bioorg Chem*, **104**, 104269. DOI: [10.1016/j.bioorg.2020.104269](https://doi.org/10.1016/j.bioorg.2020.104269).
- Faisal, H. M. N., Katti, K. S., and Katti, D. R., 2021. Binding of SARS-COV-2 (COVID-19) and SARS-COV to human ACE2: Identifying binding sites and consequences on ACE2 stiffness. *Chemical Physics*, **551**, 111353. DOI: <https://doi.org/10.1016/j.chemphys.2021.111353>.
- Frediansyah, A., Nainu, F., Dhama, K., Mudatsir, M., and Harapan, H., 2021. Remdesivir and its antiviral activity against COVID-19: A systematic review. *Clinical Epidemiology and Global Health*, **9**, 123-127. DOI: <https://doi.org/10.1016/j.cegh.2020.07.011>.
- Frisch, M., Trucks, G., Schlegel, H. B., Scuseria, G. E., Robb, M. A., Cheeseman, J. R., Scalmani, G., Barone, V., Mennucci, B., and Petersson, G., 2009. gaussian 09, Revision d. 01, Gaussian, Inc., Wallingford CT, 201.
- Gao, S., Huang, T., Song, L., Xu, S., Cheng, Y., Cherukupalli, S., Kang, D., Zhao, T., Sun, L., Zhang, J., Zhan, P., and Liu, X., 2021. Medicinal chemistry strategies towards the development of effective SARS-CoV-2 inhibitors. *Acta Pharmaceutica Sinica B*, **12**, 581-599. DOI: <https://doi.org/10.1016/j.apsb.2021.08.027>.
- Kumar, R., Kamal, R., Kumar, V., and Parkash, J., 2022. Bifunctionalization of  $\alpha,\beta$ -unsaturated diaryl ketones into  $\alpha$ -aryl- $\beta,\beta$ -ditosyloxy ketones: Single crystal XRD, DFT, FMOs, molecular electrostatic potential, hirshfeld surface analysis, and 3D-energy frameworks. *Journal of Molecular Structure*, **1250**, 131754. DOI: <https://doi.org/10.1016/j.molstruc.2021.131754>.
- Macrae, C. F., Edgington, P. R., McCabe, P., Pidcock, E., Shields, G. P., Taylor, R., Towler, M., and Van De Streek, J., 2006. Mercury: Visualization and analysis of crystal structures. *Journal of Applied Crystallography*, **39**, 453-457. DOI: [10.1107/S002188980600731X](https://doi.org/10.1107/S002188980600731X).
- Mandal, M., Chowdhury, S. K., Khan, A. A., Baidya, N., Dutta, T., Misra, D., and Ghosh, N. N., 2021. Inhibitory efficacy of RNA virus drugs against SARS-CoV-2 proteins: An extensive study. *Journal of Molecular Structure*, **1234**, 130152. DOI: <https://doi.org/10.1016/j.molstruc.2021.130152>.
- Meng, X.-Y., Zhang, H.-X., Mezei, M., and Cui, M., 2011. Molecular docking: a powerful approach for structure-based drug discovery. *Current computer-aided drug design*, **7**, 146-157. DOI: [10.2174/157340911795677602](https://doi.org/10.2174/157340911795677602).

- Morris, G. M., Huey, R., Lindstrom, W., Sanner, M. F., Belew, R. K., Goodsell, D. S., and Olson, A. J., 2009. AutoDock4 and AutoDockTools4: Automated docking with selective receptor flexibility. *Journal of computational chemistry*, **30**, 2785-2791. DOI: 10.1002/jcc.21256.
- Mueller, A. L., McNamara, M. S., and Sinclair, D. A., 2020. Why does COVID-19 disproportionately affect older people? *Aging (Albany NY)*, **12**, 9959-9981. DOI: 10.18632/aging.103344.
- Parr, R. G., 1980. Density functional theory of atoms and molecules. *Horizons of quantum chemistry*, Fukui, K., and Pullman, B. Springer, 5-15.
- Petrosillo, N., Viceconte, G., Ergonul, O., Ippolito, G., and Petersen, E., 2020. COVID-19, SARS and MERS: are they closely related? *Clinical Microbiology and Infection*, **26**, 729-734. DOI: 10.1016/j.cmi.2020.03.026.
- Raghi, K. R., Sherin, D. R., Saumya, M. J., Arun, P. S., Sobha, V. N., and Manojkumar, T. K., 2018. Computational study of molecular electrostatic potential, docking and dynamics simulations of gallic acid derivatives as ABL inhibitors. *Computational Biology and Chemistry*, **74**, 239-246. DOI: <https://doi.org/10.1016/j.compbiolchem.2018.04.001>.
- Salentin, S., Schreiber, S., Haupt, V. J., Adasme, M. F., and Schroeder, M., 2015. PLIP: fully automated protein–ligand interaction profiler. *Nucleic Acids Research*, **43**, W443-W447. DOI: 10.1093/nar/gkv315.
- Shagufta, and Ahmad, I., 2021. The race to treat COVID-19: Potential therapeutic agents for the prevention and treatment of SARS-CoV-2. *European Journal of Medicinal Chemistry*, **213**, 113157. DOI: <https://doi.org/10.1016/j.ejmech.2021.113157>.
- Sheahan, T., Sims, A., Graham, R., Menachery, V., Gralinski, L., Case, J., Leist, S., Pyrc, K., Feng, J., Trantcheva, I., Bannister, R., Park, Y., Babusis, D., Clarke, M., Mackman, R., Spahn, J., Palmiotti, C., Siegel, D., Ray, A., and Baric, R., 2017. Broad-spectrum antiviral GS-5734 inhibits both epidemic and zoonotic coronaviruses. *Science Translational Medicine*, **9**, 1-10. DOI: 10.1126/scitranslmed.aal3653.
- Sheikhpour, M., 2020. The Current Recommended Drugs and Strategies for the Treatment of Coronavirus Disease (COVID-19). *Therapeutics and clinical risk management*, **16**, 933-946. DOI: 10.2147/TCRM.S262936.
- Sheldrick, G. M., 2015. Crystal structure refinement with SHELXL. *Acta Crystallographica Section C: Structural Chemistry*, **71**, 3-8.
- Sheldrick, G. M., 2015. SHELXT - Integrated space-group and crystal-structure determination. *Acta Crystallographica Section A: Foundations of Crystallography*, **71**, 3-8. DOI: 10.1107/S2053273314026370.
- Shukla, V. K., Al-Abdullah, E. S., El-Emam, A. A., Sachan, A. K., Pathak, S. K., Kumar, A., Prasad, O., Bishnoi, A., and Sinha, L., 2014. Spectroscopic (FT-IR, FT-Raman, and UV–visible) and quantum chemical studies on molecular geometry, Frontier molecular orbitals, NBO, NLO and thermodynamic properties of 1-acetylindole. *Spectrochimica Acta Part A: Molecular and Biomolecular Spectroscopy*, **133**, 626-638. DOI: <https://doi.org/10.1016/j.saa.2014.06.043>.
- Sohag, A. A. M., Hannan, M. A., Rahman, S., Hossain, M., Hasan, M., Khan, M. K., Khatun, A., Dash, R., and Uddin, M. J., 2020. Revisiting potential druggable targets against SARS-CoV-2 and repurposing therapeutics under preclinical study and clinical trials: A comprehensive review. *Drug development research*, **81**, 919-941. DOI: 10.1002/ddr.21709.
- Srivastava, S., Ahmad, R., and Khare, S. K., 2021. Alzheimer's disease and its treatment by different approaches: A review. *European Journal of Medicinal Chemistry*, **216**, 113320. DOI: <https://doi.org/10.1016/j.ejmech.2021.113320>.
- Turner, M., McKinnon, J., Wolff, S., Grimwood, D., Spackman, P., Jayatilaka, D., and Spackman, M., 2017. CrystalExplorer17. *The University of Western Australia*, **108**, 76730.
- Westrip, S. P., 2010. PubCIF: Software for editing, validating and formatting crystallographic information files. *Journal of Applied Crystallography*, **43**, 920-925. DOI: 10.1107/S0021889810022120.
- WHO. "WHO Coronavirus (COVID-19) Dashboard." from <https://covid19.who.int/>.
- Xiang, R., Yu, Z., Wang, Y., Wang, L., Huo, S., Li, Y., Liang, R., Hao, Q., Ying, T., Gao, Y., Yu, F., and Jiang, S., 2021. Recent advances in developing small-molecule inhibitors against SARS-CoV-2. *Acta Pharmaceutica*

*Sinica B*, **12**, 1591-1623.  
<https://doi.org/10.1016/j.apsb.2021.06.016>.

DOI: Young, B., Tan, T. T., and Leo, Y. S., 2021. The place for remdesivir in COVID-19 treatment. *The Lancet Infectious Diseases*, **21**, 20-21. DOI: 10.1016/S1473-3099(20)30911-7.